Sun Glint and Sea Surface Salinity Remote Sensing

Emmanuel P. Dinnat, Paolo de Matthaeis
Goddard Earth Science and Technology Center
University of Maryland, Baltimore Campus
Baltimore, Maryland 21250

David M. Le Vine
Instrumentation Sciences Branch
Goddard Space Flight Center
Greenbelt, MD 20771

Abstract*—The Aquarius/SAC-D mission will employ three L-band (1.41 GHz) radiometers dedicated to remote sensing of Sea Surface Salinity. The mission will be in a dawn/dusk sun-synchronous orbit with the beam oriented toward the night time side of the orbit in order to limit interference from the Sun. The effect of surface roughness on solar radiation reflected from the surface will be examined. It will be shown that including the small scale roughness (waves) can have a major impact. Also, it will be shown that when the small scale waves are included it is possible to have significant radiation reflected into the main beam during seasonal extremes when a portion of the main beam is on the illuminated side of day-night terminator. *(Abstract)

Keywords-component; sea surface salinity, sun glint, L-band, Aquarius

I. INTRODUCTION

The Aquarius/SAC-D mission is dedicated to the remote sensing of Sea Surface Salinity (*SSS*) and is to be launched in 2009 [1]. An L-band (1.41 GHz) radiometer, with three beams pointing at 25.8°, 33.8° and 40.3° off the nadir, is the core instrument for retrieving *SSS*. The accuracy required on the radiometric measurements for retrieving *SSS* within the required 0.2 practical salinity unit (psu) is about 0.1 Kelvin (K). An important potential source of noise that could hinder this accuracy is the Sun. The Sun brightness temperature at L-band is three orders of magnitude larger than that of the ocean. It ranges from 100,000 K to 500,000 K depending on solar activity, whereas the ocean brightness temperature is in the range 70-110 K at the incidence angles of Aquarius. The Sun contamination is minimized by adopting a dusk/dawn (6 AM/PM equator passing times) sun-synchronous orbit, and by orienting the antenna beams towards the night side of the Earth surface (see fig. 1). Doing so, the Sun is in the direction of the antenna back lobes, where the gain is much less than at boresight, and there is no specular reflection coming through the main beam. However, contamination by reflection of the Sun radiation at the Earth surface cannot be ruled out without further investigation for two reasons.

First, even in the ideal case where the Sun is oriented at right angle with the Aquarius orbit plane, and therefore where the antennas points towards the night side, part of the antenna field of view (FOV) is over the day side. That means that Sun radiations can potentially be reflected towards the antenna side-lobes, especially under realistic assumptions for the roughness of the Earth surface.

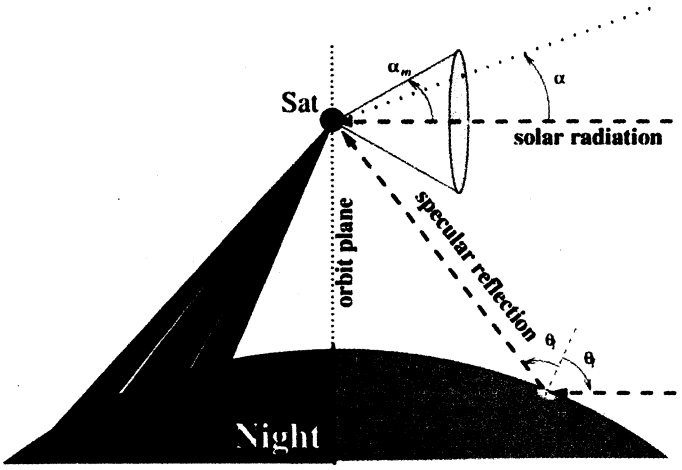

Figure 1. 2D sketch of the measurements geometry. The satellite is at the location marked Sat. The main beams of the three antenna (red in the fig.) point towards the night side of the Earth. The Sun direct radiations (upper dashed line arrow) come at right angle with the satellite orbit plane (the vertical dashed line) in this case, but can come at any elevation angle α in the cone of aperture α_m=32°. The Sun radiations specularly reflected on the Earth surface are illustrated by the lower dashed-line arrow.

Second, the satellite orbit is rarely aligned with the terminator, so in actuality, the Sun comes from various directions (illustrated by the cone of aperture α in fig. 1). When the Sun elevation increases, the illuminated area shifts towards the antenna boresights (i.e. the left side in the figure), and the antenna can point to the day side during some portions of the orbits. If the surface is rough, some Sun radiations can be scattered backward to the antenna, into the main beam.

In order to minimize contamination from L-band radiation from the Sun, the Aquarius antennas are designed to offer a gain as low as possible in the direction of the direct and (specularly) reflected radiation from the Sun (fig. 1). However, surface roughness and the associated scatter of radiation can modify the distribution of radiation coming to the antenna. The objective of this study is to quantify the impact of surface roughness on the Sun radiation reflected at the Earth surface. In section II, we describe the models employed for the reflected Sun contribution and in Section III results of numerical computations are presented comparing the geometrical optics and two scale models.

II. MODELLING INFLUENCE OF THE SUN ON THE MEASUREMENTS

A. The Geometry of the Sun contamination

We use simulations of the Aquarius orbit (JPL, personal communication) to locate the satellite in the Earth Centered Inertial (ECI) coordinate system (epoch J2000) during the year 2009 at a time resolution of 100 seconds. At each of these locations, the intersection of the antennas FOV's with the Earth surface (referred hereafter as the visible disks) are computed. We also calculate the Sun position in the ECI for the same period. The illuminated area on the Earth surface is identified, and the intersection between the visible disk and illuminated area is retained. The local incidence and azimuth angles for the Sun and the satellite are then computed over the entire illuminated visible disk. This provides the bistatic configuration for the incident and scattered radiations.

B. The surface reflectivity and the antenna temperatures

For the sake of simplification, it is assumed in this study that oceans cover the Earth surface entirely (see discussion about implications at the end of section III). The surface temperature and salinity are set to 15°C and 35 psu respectively. We compute the antenna temperature induced by the Sun radiations after reflection on the Earth surface according to three different hypotheses about the surface and the way it reflects electromagnetic waves.

First, the surface is assumed to be smooth, allowing only specular reflection obeying Fresnel's laws at the local tangent plane (the Earth surface curvature is accounted for). According to that model, there is at most one point on the Earth surface where the satellite and the Sun share the same plane of incidence and the same incidence angle with respect to the normal at the local surface. This model will be referred to as the specular point model. The Sun image antenna temperature ($T_a^{e\,I}$), according to the specular point model, is computed as

$$T_a^{e\,I} = G(\theta_{e\,I},\phi_{e\,I})R(\theta_l)T_{be}\,\Omega_e\,/4\pi \qquad (1)$$

where $\theta_{e\,I}$ and $\phi_{e\,I}$ are the spherical coordinates of the specular point in the antenna reference frame, G is the antenna gain in that direction, R is the surface Fresnel reflection coefficient, at the local incidence angle θ_l, $\Omega_e = 8.6\times10^{-5}$ sr is the Sun solid angle, assumed here to be conserved after reflection, and $T_{be} = 5\times10^5$ K is the Sun brightness temperature set large to provide an upper bound for the contamination.

Second, we account for the Sun glint induced by surface roughness. First we use a geometrical optics (*GO*) model in order to account for the tilting of the local surface due to the large-scale ocean waves. This time, contrary to the specular point model, any point on the illuminated surface can potentially reflect the Sun specularly towards the satellite if the tilt of the local surface by the waves is in the proper direction. The fraction of radiation that is reflected at each location on the illuminated surface is weighted by the probability of occurrence of the wave with the slopes required to create the specular geometry. For the probability density function (*PDF*) of the waves with slopes S_u and S_c in upwind and crosswind direction respectively, we use the zero-mean Gaussian function

$$P(S_u,S_c) = \frac{1}{2\pi\sigma_{Su}\sigma_{Sc}}\exp\left\{0.5\left[\left(\frac{S_u}{\sigma_{Su}}\right)^2+\left(\frac{S_c}{\sigma_{Sc}}\right)^2\right]\right\} \qquad (2)$$

where σ_{Su} and σ_{Sc} are the RMS of the slopes of waves with a wavelength larger than 1m. The $T_a^{e\,I}$ is then derived by integration of the weighted local reflectivity over the entire illuminated area according to

$$T_a^{e\,I} = \iint_{FOV} G(\theta,\phi)R^*(\theta_l,\phi_l)T_{be}\,\frac{\Omega_e}{4\pi}\sin\theta d\theta d\phi \qquad (3)$$

with the weighted local reflectivity

$$R^*(\theta_l,\phi_l) = R(\theta_l')\Omega_w(S_x,\theta_l)P(S_u,S_c)J(\theta,\phi) \qquad (4)$$

where θ_l' is the local incidence of the satellite and the Sun with respect to the normal of the tilted surface, $J(\theta,\phi)$ is the Jacobean determinant that converts the differential term $\sin\theta d\theta d\phi$ into $dS_u dS_c$ and $\Omega_w(S_x,\theta_l) = 1 - S_x/\tan(\theta_l)$ is the solid angle from the satellite for the wave of slope S_x in the satellite direction.

Equation (4) means that at the specular point, where the tilting required to create the specular geometry is zero, the *PDF* is maximum, and so is the weighting of the local reflection. The further from the specular point is a point in the illuminated area, the lower is the value of *PDF* at that point, and so is the weight for the reflected radiation. Basically, the reflected radiation that was concentrated in one direction with the specular point model is now spread over a broader area (which size is driven by the slopes RMS) with an exponential decrease in weighting. However, that does not mean that the local contribution given by the integrand in (3) necessarily decreases the same way as the *PDF* does, because the changes in θ_l and more importantly in antenna gain will also modulate the contribution of the individual integration points.

Finally, in the third approach, we account for all the scales of ocean waves using a two scale model (*TSM*). Here again, all the illuminated area can potentially reflect some radiation to the antenna as both scales allow fractions of radiation coming from any direction to be scattered towards any other direction. The scattering amplitude induced by the small scales is computed using the small perturbation method (*SPM*), and is modulated by the tilting induced by the large-scales [2]. That provides the two-scale reflection coefficient which is integrated over the illuminated are according to

$$T_a^{e\,I} = \iint_{FOV} G(\theta,\phi)I_{2s}T_{be}\,\sin\theta d\theta d\phi \qquad (5)$$

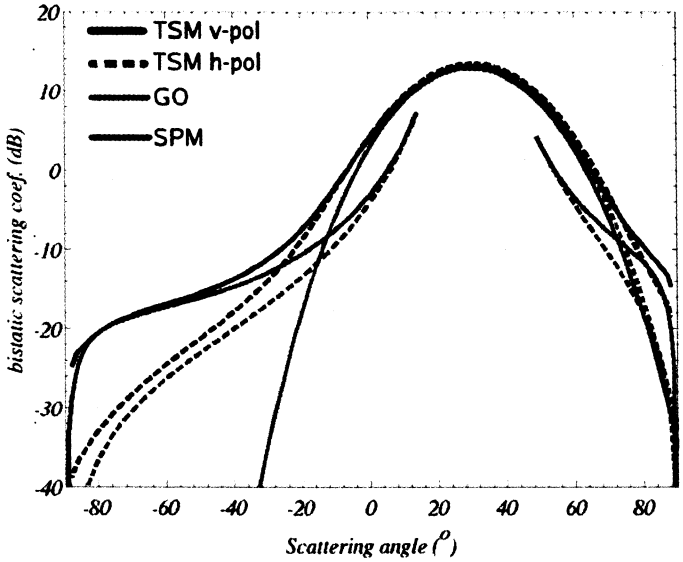

Figure 2. scattering coefficients used in the Sun glint computations (see text for models description) versus the scattering angle for an incidence angle of -30° (azimuth are the same for incident and scatted radiations). Note that the specular point model could be represented as a dirac function at scattering angle +30°. The wind speed is 8 m/s ar 10 m height.

where the two-scale reflectivity

$$I_{2s} = \iint \frac{\sigma^0(\theta_l^i, \phi_l^i; \theta_l^s, \phi_l^s)}{\cos\theta_l^s} \Omega_w P(S_u, S_c) \frac{\Omega_e}{4\pi} dS_u dS_c \quad (6)$$

is the integral over the slopes *PDF* of the *SPM* scattering coefficients $\sigma^0(\theta_l^i, \phi_l^i; \theta_l^s, \phi_l^s)$ for local incident (θ_l^i, ϕ_l^i) and scattered (θ_l^s, ϕ_l^s) directions [3] (here σ^0 is the sum of copol and crosspol term).

The scattering coefficients for the *GO* and *TSM* (R^* and I_{2s} normalized by $4\pi\cos\theta_l^s / \Omega_e$), are reported in fig. 2. Both models are relatively close around the specular direction (scattering angle +30°), but away from it, the *GO* model falls off rapidly, contrary to the *TSM*. Scattering by small scales in *h*-pol is also significantly less than in *v*-pol.

C. *The antenna gains*

We use patterns measured using a scale model of the Aquarius/SAC-D satellite (JPL, personal communication). Given the polarimetric nature of the radiometers, there are 12 gain patterns. They consist of 4 complex parameters (amplitude and phase) for each of the three beams, namely the copol and crosspol for the *v*- and *h*-pol. They are sampled at 0.5° resolution in spherical coordinates (θ, φ) (see also [4]). Fig. 3 reports the total gain (i.e. sum of the copol and crosspol gains) of the inner beam. It shows that the Sun and the specular point are located in relatively low gain areas, far from the boresight.

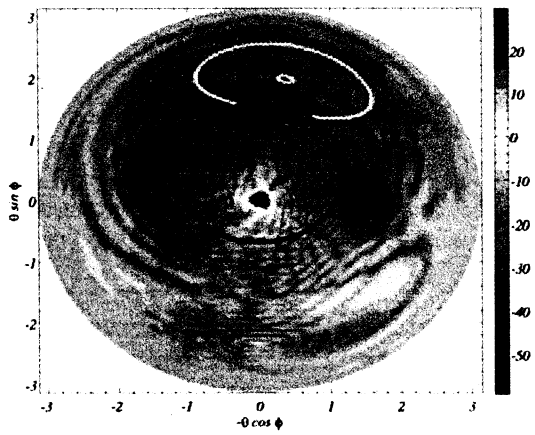

Figure 3. total gain of the inner antenna (in dB) with superimposed, the limits of the Earth FOV (black circle), and the domains in which the Sun and the specular point travel during one year (yellow and red ellipsoids respectively). The antenna boresight is at the center of the figure.

III. THE SUN INFLUENCES ON AQUARIUS MEASUREMENTS

Fig. 4 and 5 report the reflected Sun temperature versus the Sun elevation (α in fig. 1), according to the different models. Two very different situations can be identified. When the Sun elevation is low, all models predict a very small Sun contribution (less than 0.02 K for all beams, both polarizations). However, when the Sun is above the horizon (positive elevations), the Sun contribution is generally much larger than at small elevation, and some important discrepancies between the various models arise.

The dependence of the Sun image contribution on the elevation depends on the type of model used for the scattering coefficients. The results for the *GO* and *TSM* exhibit a trend in elevation whereas the specular point model appears randomly variable. The *GO* and *TSM* treat the Sun image as an extended source, and thus average the bumps and valleys of the antenna gain occurring at high spatial frequency. Consequently, the Sun image contribution follows the large trends in the antenna gain: it increases when part of the Sun image is getting close to the main beam, and remains small otherwise. The specular point model treats the Sun as a point source located at the specular point. The specular point never gets close to the main beam, and moves significantly over bumps and valleys of the antenna back lobes (fig. 3). Therefore, the contribution derived from this latter model is very variable and not noticeably dependent on the Sun elevation, but is more directly related to what particular bump or valley in the gain faces the specular point.

The *TSM* predicts the largest $T_a^{e\,I}$ of the three models at both polarizations. With this model, scattering of the Sun radiation occurs at any location on the illuminated area, towards all directions. So when the Sun elevation is large enough (around 3.5° for the inner beam, fig. 5 & 6, of the order of 6° for the outmost beam), the illuminated area drifts towards the antenna boresight and some Sun radiations are scattered backwards to enter the main beam. Even if a very small fraction of radiations is scattered (of the order of -20 dB), T_{be}

and the antenna gain prove to be large enough to induce a significant contamination in *v*-pol. It is larger than the Aquarius goal of 0.05K, during 8% of the time. Note that the results for the *v*-pol are different from those of the *h*-pol. As illustrated in

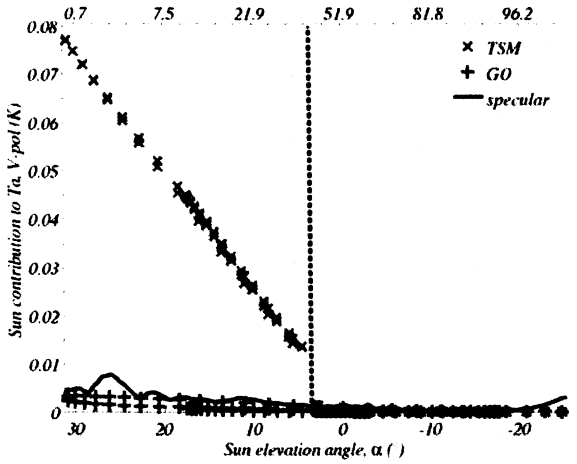

Figure 4. Sun image contribution in vertical polarization versus the Sun elevation. The vertical dashed line illustrates the elevation at which the illuminated area enters the main beam. The upper x-axis reports the cumulative percentage of Sun occurance at a given elevation angle (eg. the Sun is 21.9% of the time at elevation larger than 10°).

fig. 2, when the scattering occurs at geometries very different from the specular one, the *h*-pol scattering coefficients are much less than those in *v*-pol. Consequently, the results in *h*-pol are more similar between all models than in *v*-pol which is dominated by the small-scale contribution. Note however that the *TSM* has been found to underestimate backscattering measurements in *h*-pol by several authors.

As for the comparison of the *GO* and specular models, they predict similar order of magnitude, although the *GO* model estimate is usually less than that of the specular model, especially at very low elevations, when part of the Sun image is spread by the roughness outside of the antenna FOV. The *GO* model is relatively accurate for predicting the Sun contribution when the latter is dominated by the area near the specular point. However, when the illuminated area reaches high-gain regions (when antennas point to the illuminated side), this model dramatically underestimates the glint because of the absence of small-scale scattering,

We have also evaluated the size of the area on the surface contributing the most to $T_a^{e\ l}$ when the contamination is the most problematic (i.e. at large elevations). Most of the contribution is due to the main beam area, namely an area on the Earth surface with a diameter of the order of 200 km. This means that an accurate correction for the contamination will require information about the geophysical conditions over a limited region, which is nevertheless needed for the mission baseline. As for the simplifying hypothesis regarding the presence of land surfaces, whenever land surface is present in the main beam, contribution of the Sun image will be different from our estimates. However, the presence of land surface in some parts of the thousands of squared kilometers of the total FOV outside the main beam will likely have small impact on the results. More rigorous simulation with actual land/sea representation will be performed in the future.

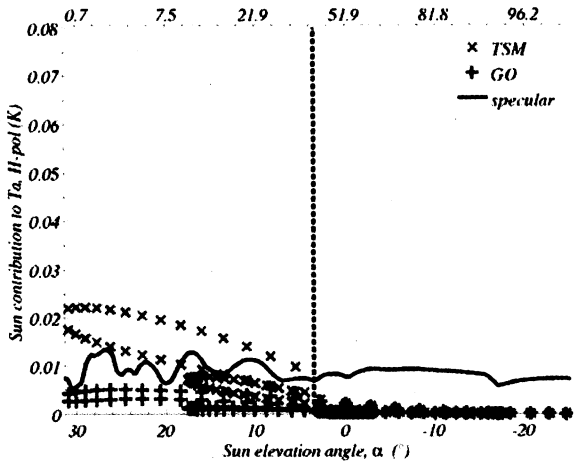

Figure 5. same as fig. 4 for the horizontal polarization.

IV. CONCLUSIONS AND PERSPECTIVE

We show that the reflection of Sun radiations from the Earth surface has to be considered in order to account properly for the Sun contamination of the Aquarius measurements. The Sun contamination after reflection on the Earth surface is small, but not always negligible if one considers the demanding accuracy needed for salinity retrieval. It is also important to account for the roughness of the surface, particularly at small scale, because it is the cause of the largest contaminations. Contamination can noticeably exceed the budgeted value of 0.05 K, especially because of the bistatic scattering allowed by the rough nature of the ocean surface. Bistatic scattering allows some radiation to reach antennas through the main beam when the antennas point to the illuminated side. Despite the fact that we have used hypotheses for a worst case scenario, and that in reality large contamination may be rare, it may be necessary to correct for this effect, at least partially. Since the surface roughness and the antenna gain will have to be very well known in the main beam direction independently of the Sun contamination issue, the constraint for an accurate Sun glint correction will be on the accuracy on the Sun brightness temperature. Future work will include simulations with a more accurate representation of the Earth surface and will also take into account the Sun brightness temperature variability.

REFERENCES

[1] D.M. Le Vine. G.S.E. Lagerloef, R. Colomb, S. Yueh, F. Pellerano, "Aquarius: An Instrument to Monitor Sea Surface Salinity from Space", IEEE Trans Geosci. & Remote Sens., submitted and revised, 2007

[2] Durden, S. L., et J. F. Vesecky, "A physical radar cross-section model for a wind-driven sea with swell", IEEE Journal of Oceanic Engineering, OE-10, 445-451, 1985.

[3] Yueh, S. H., "Modeling of wind direction signals in polarimetric sea surface brightness temperatures", IEEE Trans on Geosci. & Remote Sens, 35, 1400-1418, 1997.

[4] E. Dinnat and D.M. Le Vine, "Effects of the Antenna Aperture on Remote Sensing of Sea Surface Salinity at L-band", IEEE Trans Geosci. & Remote Sens., Special Issue on MicroRad06, accepted for publication, 2007.